First-principles calculations of x-ray absorption in a scheme based on ultrasoft pseudopotentials: From α-quartz to high-T_c compounds

Christos Gougoussis, Matteo Calandra, Ari P. Seitsonen, and Francesco Mauri
CNRS and Institut de Minéralogie et de Physique des Milieux Condensés, Case 115, 4 Place Jussieu, 75252 Paris Cedex 05, France
(Received 4 June 2009; revised manuscript received 29 June 2009; published 3 August 2009)

We develop a first-principles scheme based on the continued-fraction approach and ultrasoft pseudopotentials to calculate *K*-edge x-ray absorption spectra in solids, allowing such calculations in transition-metal and rare-earth compounds with substantially reduced cutoffs with respect to the norm-conserving case. We validate the method by calculating Si and O *K* edges in α-quartz, Cu *K* edge in copper and in La_2CuO_4. For the case of Si and O edges in α-quartz and in copper, we obtain good agreement with experimental data. In the Cu *K*-edge spectra of La_2CuO_4, a material considered a real challenge for density-functional theory, we attribute all the near-edge and far-edge peaks to single-particle excitations.

DOI: 10.1103/PhysRevB.80.075102 PACS number(s): 71.15.Dx, 71.15.Mb, 71.15.Qe

I. INTRODUCTION

With the development of synchrotron-radiation sources, x-ray absorption spectroscopy (XAS) has become a very powerful and a widely used technique to investigate structural properties and electronic structures in condensed-matter physics. Since the absorption of x rays at well-suited energies is chemical and orbital selective, it is possible to probe electronic excitations and explore the local environment around the absorbing atom. The use of polarized x rays allows to separate the contributions of different atomic orbitals through the study of angular dependence of the spectra.[1]

K-edge XAS has been used to study the electronic structure of correlated transition-metal compounds[2–4] to probe the local environment around impurities in crystals[5] and in disordered matter such as glass or liquids. For instance, XAS plays a crucial role for the understanding of the microscopic structure of water.[6–11] The widespread use of XAS as a structural utility and as a probe of the electronic structure requires reliable theoretical approaches to interpret the measured spectra.

Different theoretical methods are available to calculate XAS. The multiplet approach,[12] used to calculate pre-edge features for systems with localized final states, relies on the solution of a few-sites many-body Hamiltonian including several parameters that are suitably chosen to fit the experimental data. This approach, although providing a full many-body solution to the problem, has three main shortcomings: (i) it is limited to pre-edge structures and (ii) nonlocal excitations are hardly taken into account due to the short-range nature of the considered clusters; (iii) in some cases a small variation in the Hamiltonian parameters leads to substantially different spectra. The multiple-scattering approach[13–15] and its extension to nonmuffin-tin potentials have been widely used with success, but these methods are not based on first principles and require adjustable parameters to interpret the experimental data. The solution of the Bethe-Salpeter equation is the first principles method having the most satisfactory treatment of many-body effects.[16] However being that this method extremely time consuming it only allows for a description of the pre-edge region of the XAS spectra: the near-edge and far-edge regions cannot be easily computed.

Density-functional theory (DFT) approaches[17–22] have been successfully applied to *K* edges of weakly correlated materials. In a pseudopotential framework, the use of the projector augmented wave (PAW) (Ref. 18) method allows to reconstruct the all-electron wave function and consequently to obtain XAS intensities unaffected by the presence of a pseudopotential. Furthermore the development of a DFT method[17] using norm-conserving pseudopotentials and based on the continued-fraction approach permits to obtain XAS spectra up to the far edge region. Another advantage of DFT approaches is that they allow for structural optimization of the local environment around the absorbing atom, a key issue in the case of impurities or defects.

In time-independent DFT methods, core-hole effects are included in a supercell approach by generating a pseudopotential with a core hole in the desired atomic core level. While this method works very well for weakly correlated system, in the presence of moderate or strong correlation it has two main shortcomings. The first is the unsatisfactory treatment of electron-electron interaction in the DFT functional. The second is the large increase in computational time when dealing with transition metals and rare earths mainly related to the huge kinetic-energy cutoffs involved and the need to simulate large supercells with reduced symmetry.[23] A partial remedy for the lack of correlation effects is the use of the DFT+U approximation.[24] Recently the method of Ref. 17 was generalized to the DFT+U approximation.[4] It was shown the DFT+U dramatically improves the agreement with experimental data in the pre-edge region of correlated 3*d* transition-metal compounds.[4] Still the second problem holds, namely, the huge cutoffs needed to simulate transition-metal and rare-earth compounds require a substantial computational time.

In this work we solve this problem by developing a method to calculate XAS in an ultrasoft (US) pseudopotential[25] scheme and relying on the continued-fraction approach. US pseudopotentials allow for low cutoffs (20–40 Ry) even for transition metals and rare-earth systems, contrary to norm-conserving ones. Thus the use of these pseudopotentials reduces the computational cost of the supercell calculation by one order of magnitude. The drawback is that the continued-fraction scheme developed in Ref. 17

does not apply if at least one ultrasoft pseudopotential (not necessary the absorbing atom) is present in the calculation. For this reason we reformulate completely the continued fraction and the corresponding Lanczos approach in a way that is suitable for ultrasoft pseudopotentials. We then apply the method to Si and O K edges in α-quartz, to Cu K edge in copper, and in La_2CuO_4 and compare the results with available experimental data.

The structure of the paper is as follows. In Secs. II and III we remind the general expression of the XAS cross section within the projector augmented wave formalism. In Secs. IV and V we develop the continued-fraction approach in the case of ultrasoft pseudopotentials, and finally in Sec. VI we apply the method to the aforementioned systems.

II. X-RAY ABSORPTION CROSS SECTION

The XAS cross section is[1]

$$\sigma(\omega) = 4\pi^2 \alpha \hbar \omega \sum_f |M_{i\to f}|^2 \delta(E_f - E_i - \hbar\omega), \tag{1}$$

where $\hbar\omega$ is the incident photon energy, α is the fine-structure constant, and $M_{i\to f}$ is the transition amplitude between the initial state $|\psi_i\rangle$ of energy E_i and the final state $|\psi_f\rangle$ of energy E_f. In a single-particle approach, the many-body $|\psi_i\rangle$ and $|\psi_f\rangle$ are replaced by single-particle states. Since we consider K and L_1 edges, $|\psi_i\rangle$ can be either the $1s$ or the $2s$ atomic core state in the absence of a core hole. The final state $|\psi_f\rangle$ in the presence of a core hole is obtained in an all-electron first principles calculation.

In a single-particle approach and in the electric-quadrupole approximation, the transition amplitude is given by the matrix element

$$M_{i\to f} = \langle \psi_f | \mathcal{D} | \psi_i \rangle \tag{2}$$

with

$$\mathcal{D} = \hat{\epsilon}\cdot\mathbf{r} + \frac{i}{2}(\hat{\epsilon}\cdot\mathbf{r})(\mathbf{k}\cdot\mathbf{r}), \tag{3}$$

where $\hat{\epsilon}$ and $\mathbf{k}$ are the polarization vector and the wave vector of the incident beam and $\mathbf{r}$ is the electron coordinate.

III. X-RAY ABSORPTION CROSS SECTION IN A PAW FORMALISM

In a first principles pseudopotential approach, the calculated wave function is $|\tilde{\psi}_f\rangle$, namely, the pseudowave function of the crystal obtained at the end of the self-consistent field run. In order to get the all-electron wave functions $|\psi_f\rangle$ needed in Eqs. (1) and (3), all-electron reconstruction needs to be performed. This is achieved in the framework of the PAW method.[18] In this approach the all-electron wave functions $|\psi\rangle$ are related to the pseudowave functions $|\tilde{\psi}\rangle$ though the linear operator $\mathcal{T}$,

$$|\psi\rangle = \mathcal{T}|\tilde{\psi}\rangle. \tag{4}$$

The $\mathcal{T}$ operator is written as a sum of local contributions centered around each atomic site $\mathbf{R}$,

$$\mathcal{T} = 1 + \sum_{\mathbf{R}} \mathcal{T}_{\mathbf{R}}. \tag{5}$$

The local operators $\mathcal{T}_{\mathbf{R}}$ act only within the so-called augmentation regions $\Omega_{\mathbf{R}}$ centered on atomic sites. Following Ref. 18, we introduce the all-electron (pseudo) partial waves $|\phi_{\mathbf{R},n}\rangle$ ($|\tilde{\phi}_{\mathbf{R},n}\rangle$) and the projector functions $\langle\tilde{p}_{\mathbf{R},n}|$ that satisfy the conditions[26]

$$\tilde{\phi}_{\mathbf{R},n}(\mathbf{r}) = \phi_{\mathbf{R},n}(\mathbf{r}) \quad \text{outside} \quad \Omega_{\mathbf{R}}, \tag{6}$$

$$\langle \tilde{p}_{\mathbf{R},n} | \tilde{\phi}_{\mathbf{R}',n'} \rangle = \delta_{\mathbf{R}\mathbf{R}'}\delta_{nn'}. \tag{7}$$

The wave functions $|\phi_{\mathbf{R},n}\rangle$ and $|\tilde{\phi}_{\mathbf{R},n}\rangle$, respectively, form a basis for valence states, which means that any function $\chi_{\mathbf{R}}$ that vanishes outside Ω_R is expanded as

$$\sum_n |\tilde{p}_{\mathbf{R},n}\rangle\langle\tilde{\phi}_{\mathbf{R},n}|\chi_{\mathbf{R}}\rangle = |\chi_{\mathbf{R}}\rangle. \tag{8}$$

Then the operator $\mathcal{T}$ is written as

$$\mathcal{T} = 1 + \sum_{\mathbf{R},n} (|\phi_{\mathbf{R},n}\rangle - |\tilde{\phi}_{\mathbf{R},n}\rangle)\langle\tilde{p}_{\mathbf{R},n}|. \tag{9}$$

Substituting Eq. (9) in Eq. (4) and Eq. (4) in Eq. (2) leads to

$$M_{i\to f} = \langle\tilde{\psi}_f|\mathcal{D}|\psi_i\rangle + \sum_{\mathbf{R},n} \langle\tilde{\psi}_f|\tilde{p}_{\mathbf{R},n}\rangle\langle\phi_{\mathbf{R},n}|\mathcal{D}|\psi_i\rangle - \sum_{\mathbf{R},n} \langle\tilde{\psi}_f|\tilde{p}_{\mathbf{R},n}\rangle\langle\tilde{\phi}_{\mathbf{R},n}|\mathcal{D}|\psi_i\rangle. \tag{10}$$

Since the initial wave function ψ_i is localized on the absorbing atom (located at $\mathbf{R}_0$), the terms having $\mathbf{R} \neq \mathbf{R}_0$ can be neglected in Eq. (10) to obtain

$$M_{i\to f} = \langle\tilde{\psi}_f|\tilde{\phi}_{\mathbf{R}_0}\rangle \tag{11}$$

with

$$|\tilde{\phi}_{\mathbf{R}_0}\rangle = \sum_n |\tilde{p}_{\mathbf{R}_0,n}\rangle\langle\phi_{\mathbf{R}_0,n}|\mathcal{D}|\psi_i\rangle. \tag{12}$$

Replacing this matrix element in the XAS cross section leads to

$$\sigma(\omega) = 4\pi^2\alpha\hbar\omega\sum_f |\langle\tilde{\psi}_f|\tilde{\phi}_{\mathbf{R}_0}\rangle|^2 \delta(E_f - E_i - \hbar\omega). \tag{13}$$

Thus Eq. (13) expresses the XAS cross section in terms of single-particle states obtained from a pseudopotential calculation. Note that in Eq. (12) there is an infinite number of projectors. Practically only a few projectors are needed to achieve convergence.

IV. XAS IN AN ULTRASOFT PSEUDOPOTENTIAL SCHEME

In an ultrasoft scheme the norm of the pseudopartial waves is different from the norm of the corresponding all-electron partial waves. For this reason it is customary to define[27] the integrated augmentation charges $q_{\mathbf{R},\mathbf{nm}}$ as

$$q_{\mathbf{R},nm} = \langle \phi_{\mathbf{R},n} | \phi_{\mathbf{R},m} \rangle - \langle \tilde{\phi}_{\mathbf{R},n} | \tilde{\phi}_{\mathbf{R},m} \rangle. \quad (14)$$

The S operator defined in the ultrasoft scheme[25] is then

$$S = \mathbb{1} + \sum_{\mathbf{R},m,n} |\tilde{p}_{\mathbf{R}n}\rangle q_{\mathbf{R},nm} \langle \tilde{p}_{\mathbf{R}m}| = \mathbb{1} + \sum_{\mathbf{R}} Q_{\mathbf{R}}. \quad (15)$$

The pseudo-Hamiltonian $\tilde{H}$ and the pseudoeigenfunctions $|\tilde{\psi}_f\rangle$ satisfy the following equation:[25]

$$\tilde{H}|\tilde{\psi}_f\rangle = E_f S |\tilde{\psi}_f\rangle. \quad (16)$$

Multiplication of Eq. (16) by $S^{-1/2}$ leads to

$$S^{-1/2}\tilde{H}S^{-1/2}S^{1/2}|\tilde{\psi}_f\rangle = E_f S^{1/2}|\tilde{\psi}_f\rangle. \quad (17)$$

The following identity holds (for proof see Appendix A):

$$\pi \sum_f |\tilde{\psi}_f\rangle \delta(E_f - x) \langle \tilde{\psi}_f| = \lim_{\gamma \to 0} \Im[\tilde{G}(x)], \quad (18)$$

where x is a real number and

$$\tilde{G}(x) = S^{-1/2} \frac{1}{x - S^{-1/2}\tilde{H}S^{-1/2} - i\gamma} S^{-1/2}. \quad (19)$$

Using Eqs. (13) and (18), the XAS cross section can finally be written in a suitable form for a standard Lanczos procedure,

$$\sigma(\omega) = 4\pi\alpha\hbar\omega \lim_{\gamma \to 0} \Im[\langle \tilde{\phi}_{\mathbf{R}_0} | \tilde{G}(\hbar\omega + E_i) | \tilde{\phi}_{\mathbf{R}_0} \rangle], \quad (20)$$

where E_i is the energy of the initial state that in a pseudopotential scheme is determined up to an overall constant. In the case of a unit cell having multiple absorbing sites, which are equivalent under the point-group symmetry of the crystal, E_i is the same for all the absorbing atoms and the choice of E_i simply corresponds to a rigid shift in the overall spectrum. On the contrary, in the case of nonequivalent absorbing sites in the unit cell, the value of E_i depends on the absorbing site due to the core-level shift. In this case the choice of E_i is not arbitrary and careful determination of the core-level shift is needed.[22] For simplicity in this work we consider only examples in which there are only equivalent absorbing sites in the unit cell. The determination of the core-level shift in the case of multiple nonequivalent absorbing sites will be given elsewhere. Thus in what follows we choose the energy E_i to be the Fermi level, in the metallic case, the highest occupied state, in the insulating case.

V. LANCZOS PROCEDURE

Equation (20) can be calculated using the Lanczos recursion method.[28–31] The quantity $\langle \tilde{\phi}_{\mathbf{R}_0} | \tilde{G}(E_i + \hbar\omega) | \tilde{\phi}_{\mathbf{R}_0} \rangle$ is evaluated using the continued fraction,

$$\langle \tilde{\phi}_{\mathbf{R}_0} | \tilde{G}(E) | \tilde{\phi}_{\mathbf{R}_0} \rangle = \cfrac{\langle \tilde{\phi}_{\mathbf{R}_0} | S^{-1} | \tilde{\phi}_{\mathbf{R}_0} \rangle}{a_0 - E - i\gamma - \cfrac{b_1^2}{a_1 - E - i\gamma - \cfrac{b_2^2}{\ddots}}}, \quad (21)$$

where the real numbers a_i and b_i are computed recursively by defining the vectors $|u_i\rangle$ such that

$$|u_0\rangle = \frac{S^{-1/2}|\tilde{\phi}_{\mathbf{R}_0}\rangle}{\sqrt{\langle \tilde{\phi}_{\mathbf{R}_0} | S^{-1} | \tilde{\phi}_{\mathbf{R}_0} \rangle}},$$

$$S^{-1/2}\tilde{H}S^{-1/2}|u_i\rangle = a_i|u_i\rangle + b_{i+1}|u_{i+1}\rangle + b_i|u_{i-1}\rangle.$$

The a_i and b_i coefficients are defined as

$$a_i = \langle u_i | S^{-1/2}\tilde{H}S^{-1/2} | u_i \rangle, \quad (22)$$

$$b_i = \langle u_i | S^{-1/2}\tilde{H}S^{-1/2} | u_{i-1} \rangle. \quad (23)$$

This is essentially a standard Lanczos process where the initial vector is $|u_0\rangle$ and the Hamiltonian $\tilde{H}$ is replaced by $S^{-1/2}\tilde{H}S^{-1/2}$. However this is not the more efficient way to carry out the Lanczos chain since two multiplications by $S^{-1/2}$ are involved and the S matrix is of the same order as the Hamiltonian, namely, the dimension is given by the number of plane waves in the calculation (the kinetic-energy cutoff). Thus any application of $S^{-1/2}$ costs as much as the application of $\tilde{H}$.

A more efficient way to implement the Lanczos process is obtained by defining the auxiliary vectors $|t_i\rangle$, namely,

$$|t_i\rangle = S^{1/2}|u_i\rangle. \quad (24)$$

Using this definition, the Lanczos process can now be directly carried out on the $|t_i\rangle$ vectors as

$$|t_0\rangle = \frac{|\tilde{\phi}_{\mathbf{R}_0}\rangle}{\sqrt{\langle \tilde{\phi}_{\mathbf{R}_0} | S^{-1} | \tilde{\phi}_{\mathbf{R}_0} \rangle}},$$

$$\tilde{H}S^{-1}|t_i\rangle = a_i|t_i\rangle + b_{i+1}|t_{i+1}\rangle + b_i|t_{i-1}\rangle,$$

where the new Lanczos vectors $|t_i\rangle$ are no longer orthogonal but $\langle t_i | S^{-1} | t_j \rangle = \delta_{i,j}$. If during the Lanczos chain the vectors $|\tilde{t}_i\rangle = S^{-1}|t_i\rangle$ are stored then the a_i and b_i coefficients can be defined as

$$a_i = \langle \tilde{t}_i | \tilde{H} | \tilde{t}_i \rangle, \quad (25)$$

$$b_i = \langle \tilde{t}_i | \tilde{H} | \tilde{t}_{i-1} \rangle, \quad (26)$$

Now, each iteration needs only one multiplication by S^{-1}, one multiplication by $\tilde{H}$, and four Lanczos vectors stored in memory, namely, $|t_{i-1}\rangle$, $|\tilde{t}_{i-1}\rangle$, $|t_i\rangle$ and $|\tilde{t}_i\rangle$.

To achieve an efficient implementation of the Lanczos process, particular care needs to be taken in inverting the S matrix to calculate S^{-1}. Direct inversion of the S matrix is unfeasible being the order of the matrix given by the number of plane waves. Using the definition of S in terms of the N_p ultrasoft projectors, the calculation of S^{-1} can be performed very efficiently by simple products and inversions of matrices of the order of $N_p \times N_P$, as it was demonstrated in Refs. 32 and 33. In order to have a complete description of the method used we recall the main passages of the demonstration of Refs. 32 and 33 in Appendix B.

VI. APPLICATIONS

The developed method is now applied to silicon and oxygen K edges in α-quartz and to Cu K edge in copper and in La_2CuO_4. Density-functional theory calculations are performed using the Quantum ESPRESSO package[34] and the generalized gradient approximation (GGA).[35] In the case of La_2CuO_4 we use the spin polarized generalized gradient approximation. The developed continued-fraction approach to deal with US pseudopotentials is implemented in the XSPECTRA package[36] and distributed with the current developmental version of the Quantum ESPRESSO code. Occupied states are eliminated from the spectrum using the method of Ref. 37. The zero of energy is determined from the self-consistent calculation on a supercell in the presence of a core hole. In the metallic case we chose the Fermi level while in the insulating case the highest occupied state. It is important to notice that an insulator can become metallic in the supercell calculation due to core-hole attraction. In this case the elimination of the occupied states is somewhat ill defined, as it is in metallic systems. When this occurs, the pre-edge features can be incorrect. This is the case in La_2CuO_4. Further technical details of the calculations are given in each subsection.

A. SiO_2 (α-quartz)

SiO_2 (α-quartz) is a dichroic compound with a hexagonal unit cell and lattice parameters a=4.9141 Å and c =5.4060 Å.[38] The dipolar cross section σ has the following angular dependence:[1]

$$\sigma(\epsilon) = \cos^2(\theta)\sigma_{\parallel} + \sin^2(\theta)\sigma_{\perp}, \tag{27}$$

where ϵ is the polarization vector and θ is the angle between the c axis and ϵ.

The charge-density calculation was performed with a $2\times2\times2$ supercell containing 72 atoms. Electronic integration was performed using only the Γ point. We used a 20 Ry kinetic-energy cutoff and a 150 Ry cutoff for the charge density to be compared to the 70 Ry kinetic-energy cutoff needed in a standard norm-conserving pseudopotentials calculation.[17] The electronic integration in the continued-fraction calculation using the Lanczos method was performed using a centered $3\times3\times3$ **k**-points grid of the 72 atoms supercell. Two projectors per channel were used in the PAW reconstruction. The core-hole width was taken constant and set to 0.8 eV for Si K edge and 1 eV for O K edge. The continued-fraction calculation needed around 400 iterations per **k** point. We performed a calculation with norm-conserving pseudopotentials in which around 600 iterations were needed for comparable accuracy, such as in previous work.[1] Thus the number of iterations needed is smaller due to the smaller cutoff energy.

Our results are presented in Figs. 1 and 2. These results are in perfect agreement with those presented in Ref. 17 and obtained with norm-conserving pseudopotentials. The experimental Si k-edge XAS cross section is very well reproduced for both polarizations despite a too-weak peak around 7 eV. Good agreement between theory and experiment for O K edge is obtained.

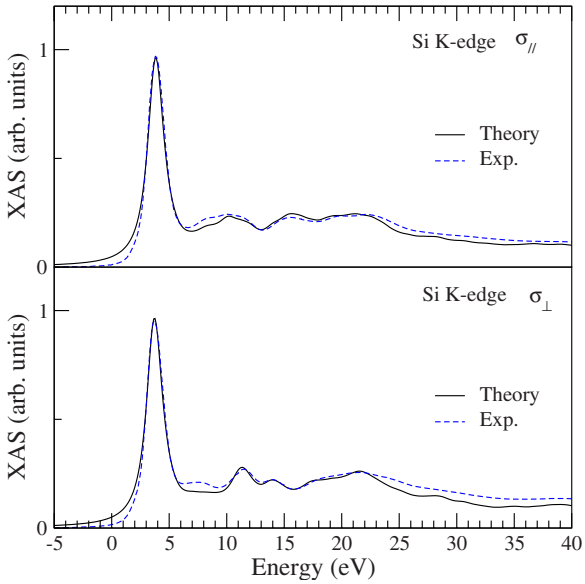

FIG. 1. (Color online) Experimental (Ref. 17) and calculated Si K edge in α-quartz. $\sigma_{\parallel}$ is the polarization along the c axis, while $\sigma_{\perp}$ is the in-plane polarization.

The comparison between the ultrasoft pseudopotential and the norm-conserving pseudopotential calculations on α-quartz validates our implementation of XAS using ultrasoft pseudopotentials.

B. Copper

Pure copper at room temperature crystallizes in the fcc structure with lattice parameter 3.601 Å.[39] The copper K-edge XAS cross section was calculated on a converged $3\times3\times3$ supercell containing 27 atoms. Electronic integration was performed over a $10\times10\times10$ uniform k-point grid for

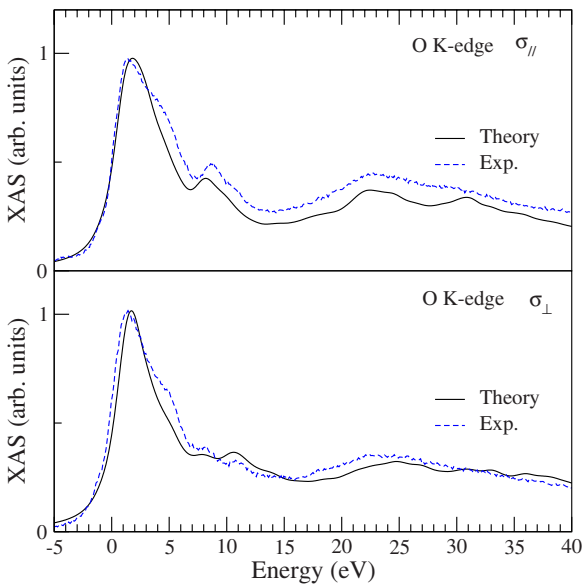

FIG. 2. (Color online) Experimental (Ref. 17) and calculated O K edge in α-quartz. $\sigma_{\parallel}$ is the polarization along the c axis, while $\sigma_{\perp}$ is the in-plane polarization.

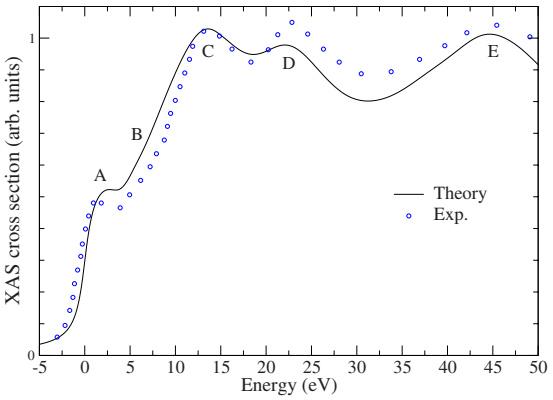

FIG. 3. (Color online) Calculated Cu K edge in copper compared to experimental data from Ref. 40. The Lorentzian γ broadening parameters vary and run from 1 to 4 eV.

both charge density and XAS calculations, with a 30 Ry kinetic-energy cutoff and a 500 Ry charge-density cutoff.

The calculated XAS cross section is in good agreement with experimental data (Fig. 3). Features A, B, C, D, and E are correctly reproduced; however, peak A (shoulder) is shifted about 1 eV to higher energies. This shift is also present in finite difference method calculations.[41] Since copper is metallic, the description of the A peak is difficult because the core-hole attraction can drag some states below the Fermi energy.

C. La_2CuO_4

La_2CuO_4 is the parent compound of high-T_c superconductors. It is an antiferromagnetic correlated insulator considered as a challenge for density-functional theory. Furthermore it requires large cutoff energies to be simulated with norm-conserving pseudopotentials. Thus it is an ideal test for our approach.

At low temperatures La_2CuO_4 present a weak orthorhombic distortion of the tetragonal structure. In our calculation we neglect the orthorhombic distortion and consider the tetragonal structure having $a=5.357$ Å and $c=13.143$ Å.[42] Under this assumption, the Cu K-edge XAS dipolar cross section can be described as a linear combination of the cross section having in-plane polarization ($\sigma_\perp$) and of that having polarization along the c axis ($\sigma_\parallel$), as expressed in Eq. (27).

We treat correlation effects as the framework of the spin-polarized GGA+U (Refs. 35 and 43) approximation, where U is the Hubbard parameter on Cu $3d$ states. The U parameter is 9.6 eV, as calculated from first principles using a linear-response scheme.[43,44] We use ultrasoft pseudopotentials for all atomic species leading to a 30 Ry kinetic-energy cutoff and a 200 Ry charge-density cutoff. The kinetic-energy cutoff used with ultrasoft pseudopotentials has to be compared with the more than 150 Ry kinetic-energy cutoff needed in the case of norm-conserving pseudopotentials. We use two PAW projectors per channel and nonlinear core correction in the Cu pseudopotential. By calculating XAS on the antiferromagnetic unit cell we have checked that the inclusion of semicore states does not affect the result. We used a $1\times1\times1$ supercell of the antiferromagnetic crystal cell containing 14 atoms. For the electronic integration we use a uniform $6\times6\times6$ k-point mesh both for the charge density and for the continued-fraction calculation. We have verified that the result is unaffected by the use of larger supercells.

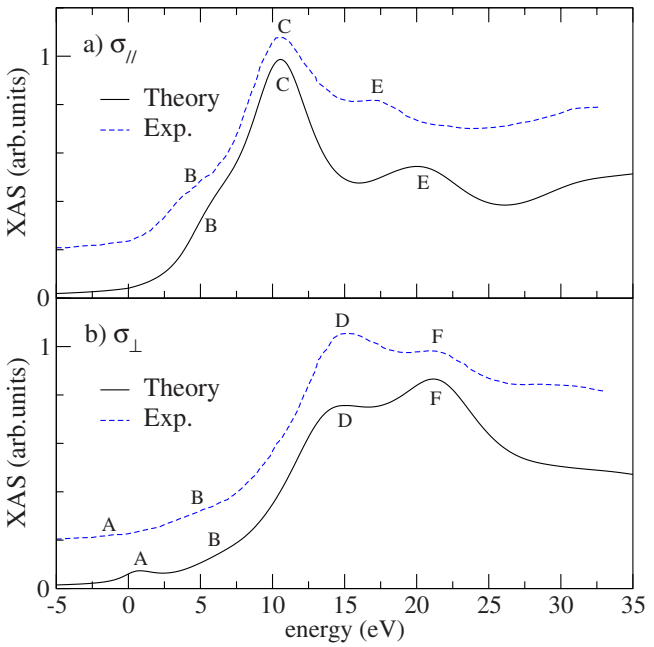

FIG. 4. (Color online) Experimental (Ref. 47) and calculated Cu K edge in La_2CuO_4. The calculated cross section was obtained with a $U=9.6$ eV parameter on Cu $3d$ states. The Lorentzian γ broadening parameters vary linearly between 1 eV in the pre-edge region and 4 eV in the far-edge region. $\sigma_\parallel$ indicates the polarization along the c axis, while $\sigma_\perp$ is the in-plane one.

Experimentally, La_2CuO_4 is an insulator with a gap around 2 eV (Ref. 45) and exhibits an antiferromagnetic order[46] with a magnetic momentum on copper atoms around $0.5\mu_B$. Our GGA+U electronic structure calculation gives a 0.5 eV charge-transfer gap and a magnetization of $0.58\mu_B$.

The results of the GGA+U Cu K edge XAS calculations are presented in Fig. 4. When the polarization is parallel to the CuO_2 planes the energy position of the different peaks is well reproduced by our calculation. In particular B, D, and F are at the correct energy position; however; the intensity of peak D is underestimated. In the pre-edge region peak A is shifted to higher energy. The A peak is not well described in our calculation since, due to the underestimation of the electronic gap and overestimation of core-hole attraction, the system becomes metallic when a core hole is included in the calculation. In particular, while the system in the absence of a core hole is insulating, when we add the core hole in the supercell calculation, we obtain a metallic system. As a consequence it becomes impossible to distinguish between occupied and empty states. The intensity of peak A is crucially affected. The system is formally in a $|3d^{10}\underline{L}\rangle$ state with no empty d states and consequently no quadrupolar pre-edge. On the contrary it is known that a weak quadrupolar pre-edge is present in experiments.[3]

The nature of peak B has been widely discussed. It has been alternatively assigned to shake down $1s^23d^9L \rightarrow 1s^13d^{10}\underline{L}$ processes[48] and to empty p states of the absorb-

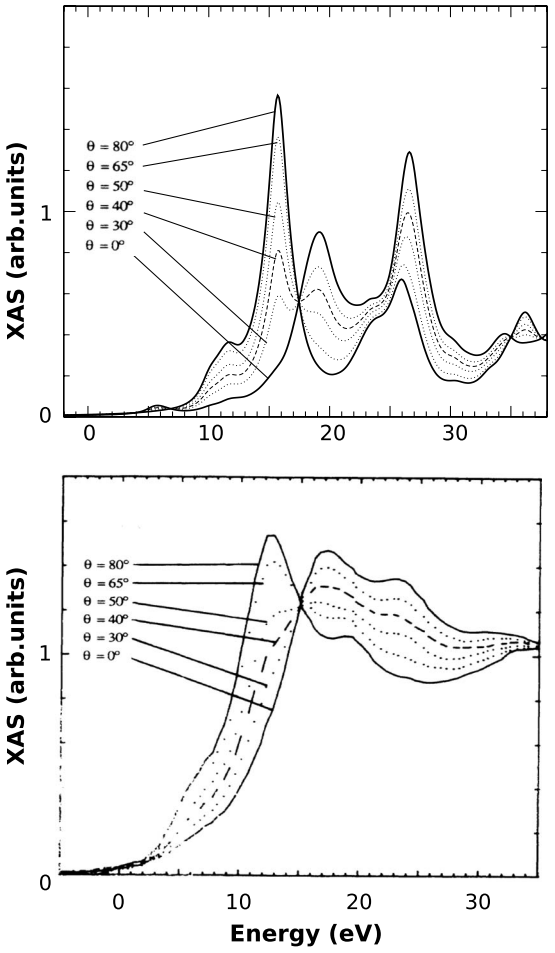

FIG. 5. Angular dependence of La_2CuO_4 Cu *K*-edge XAS dipolar cross section compared with experimental data (Ref. 47). The angle between the CuO_2 layer and the *c* axis is labeled θ so that $\theta=90°$ corresponds to ϵ along the *c* axis. The Lorentzian γ broadening parameter is 0.8 eV. The core-hole width has been artificially reduced in the calculation to show the presence of different peaks.

ing atom.[47,49] Here we unambiguously attribute peak B to empty *p* states and thus this excitation is single particle in nature.

In the spectra having polarization along the *c* axis the intensities are in better agreement with experimental data. However peak E is substantially shifted to higher energies (3 eV). More insight on this issue can be obtained by considering the angular dependence of the spectra and by comparing it to available experimental data,[47] as shown in Fig. 5.

In the theoretical calculation of Fig. 5 we have substantially reduced the peak linewidth to 0.8 eV to emphasize the multistructured form of the different peaks. In particular it is seen that the peak at 20 eV (labeled peak E in Fig. 4) is actually composed of two different peaks. The high-energy one is at the correct energy position, while the low-energy one is shifted to higher energy with respect to the experiment. The incorrect position of the lowest-energy peak substantially affects the intensity in the 10–20 eV region for both polarizations and is responsible for the disagreement with the experimental data. Indeed if this peak was at low energy the intensity of peak D in Fig. 4 would also increase and better agreement with experiment would be obtained for both polarizations.

Kosugi *et al.*[49] attributed the doubling of pre-edge and near-edge features present in *K*-edge XAS on powder samples to charge-transfer multideterminant effects. In particular it was shown that the main edge and the B peak are doubled in the isotropic spectra. However the pre-edge and edge structures occur at different energies when the polarization is in the plane or out of plane. We find that the doubling indeed originates from the average over different polarization of the single-particle spectra. Thus the doubling of edge and pre-edge peaks is not due to multideterminant charge-transfer effects.

Tolentino *et al.*[47] assigned peaks C and E to $3d^{10}\underline{L}$ transitions and peaks D and F to $3d^{9}L$ transitions, implying that the XAS spectrum includes multideterminant effects. If this would be the case, being that our calculation is single determinant in nature, a single peak should be seen in both directions. This is however not the case and our calculation correctly reproduces the main experimental features except for an energy shift for peak E. Consequently the near-edge and far-edge structures detected in *K* edge XAS of La_2CuO_4 are all single particle in origin. Concerning the E peak, it corresponds to a single-particle excitation that is 3 eV shifted with respect to experiments. This shift can be due to an incorrect description of the hybridization between Cu 4*p* states of the absorbing atom and La states. La states are indeed hard to describe in a single-particle approach for their intrinsic correlated nature. We believe that, despite the 3 eV shift of the E-peak, the single-particle origin of the C, D, E, and F peaks is definitely clarified. To have better insight on the subject it would be interesting to study the case of $Ca_{2-x}CuO_2Cl_2$ (Ref. 50) since no rare earths are present in the system and consequently the E peak should be at the right position.

VII. CONCLUSION

A DFT-based continued-fraction method using ultrasoft pseudopotentials to calculate the x-ray absorption spectra is presented. Our implementation, relying on ultrasoft pseudopotentials, is 1 order of magnitude faster than preceding implementations based on norm-conserving one.[4,17] Indeed the bulk of the calculation is the determination of the self-consistent charge density for a supercell in the presence of a core hole. Since ultrasoft pseudopotentials allow for substantially smaller cutoffs, the computation cost is strongly reduced. Furthermore the number of iteration in the continued fraction is reduced and convergence is then faster than the norm-conserving case.

We validate the method by calculating silicon and oxygen *K* edges of alpha-quartz, Cu *k* edge in bulk metallic copper and Cu *K* edge in La_2CuO_4. In the case of weak to intermediate correlation (silicon and oxygen *K* edges of alpha-quartz and Cu *K* edge in metallic copper) we obtain good agreement with experimental data. The description of XAS spectra of strongly correlated compounds as La_2CuO_4 is typically considered a challenge for DFT-based method. Nevertheless we were able to attribute all the single-particle peaks (B, C, D, and F in Fig. 4). We then solve the long-standing[47–49] discus-

sion on the attribution of the near-edge and far-edge features in La_2CuO_4.

ACKNOWLEDGMENTS

We acknowledge fruitful discussions with A. M. Saitta, R. Gebauer, D. Cabaret, Ch. Brouder, Ph. Sainctavit, N. Marzari, and D. Ceresoli. Calculations were performed at the IDRIS supercomputing center (Project No. 081202).

APPENDIX A: PROOF OF Eq. (18)

We proof that for x real number the following holds:

$$\pi\sum_f |\tilde{\psi}_f\rangle\delta(E_f-x)\langle\tilde{\psi}_f| = \lim_{\gamma\to 0}\Im\left[S^{-1/2}\frac{1}{x-S^{-1/2}\tilde{H}S^{-1/2}-i\gamma}S^{-1/2}\right]. \tag{A1}$$

Since

$$\pi\sum_f |\tilde{\psi}_f\rangle\delta(E_f-x)\langle\tilde{\psi}_f| = \lim_{\gamma\to 0}\Im\left[\sum_f |\tilde{\psi}_f\rangle\frac{1}{x-E_f-i\gamma}\langle\tilde{\psi}_f|\right], \tag{A2}$$

we have

$$\sum_f |\tilde{\psi}_f\rangle\frac{1}{x-E_f-i\gamma}\langle\tilde{\psi}_f| = \sum_f S^{-1/2}\frac{1}{x-E_f-i\gamma}S^{1/2}|\tilde{\psi}_f\rangle\langle\tilde{\psi}_f| = \sum_f S^{-1/2}\frac{1}{x-S^{-1/2}\tilde{H}S^{-1/2}-i\gamma}S^{1/2}|\tilde{\psi}_f\rangle\langle\tilde{\psi}_f|$$
$$= S^{-1/2}\frac{1}{x-S^{-1/2}\tilde{H}S^{-1/2}-i\gamma}S^{-1/2}\sum_f S|\tilde{\psi}_f\rangle\langle\tilde{\psi}_f| = S^{-1/2}\frac{1}{x-S^{-1/2}\tilde{H}S^{-1/2}-i\gamma}S^{-1/2},$$

where in the last equality we used the following property:[25]

$$\mathbb{1} = \sum_f |\tilde{\psi}_f\rangle\langle\tilde{\psi}_f|S = \sum_f S|\tilde{\psi}_f\rangle\langle\tilde{\psi}_f|. \tag{A3}$$

Equation (A1) follows from Eq. (A3).

APPENDIX B: CALCULATING THE S^{-1} MATRIX

Following Ref. 25, the S matrix can be written as

$$S = \mathbb{1} + \sum_{i,j} q_{ij}|\tilde{p}_i\rangle\langle\tilde{p}_j|, \tag{B1}$$

where i and j are cumulative indexes for $\mathbf{R}m$ and $\mathbf{R}n$, respectively. We assume that S^{-1} can be written as

$$S^{-1} = \mathbb{1} + \sum_{i,j} a_{ij}|\tilde{p}_i\rangle\langle\tilde{p}_j|. \tag{B2}$$

The S^{-1} matrix satisfies the equation $SS^{-1}=\mathbb{1}$,

$$SS^{-1} = \left(\mathbb{1} + \sum_{i,j} q_{ij}|\tilde{p}_i\rangle\langle\tilde{p}_j|\right)\left(\mathbb{1} + \sum_{l,m} a_{lm}|\tilde{p}_l\rangle\langle\tilde{p}_m|\right)$$
$$= \mathbb{1} + \sum_{i,j}|\tilde{p}_i\rangle\langle\tilde{p}_j|\left(q_{ij} + a_{ij} + \sum_{lm} q_{ij}P_{jl}a_{lm}\right), \tag{B3}$$

where $P_{jl}=\langle\tilde{p}_j|\tilde{p}_l\rangle$. In matrix form the equation is

$$q + a + qPa = 0, \tag{B4}$$

whose solution is $a=-(1+qP)^{-1}Q$. Thus S^{-1} can be calculated by inverting matrices of the size of $N_P\times N_P$, where N_P is the number of ultrasoft projectors. A similar procedure was used in Refs. 32 and 33.

[1] C. Brouder, J. Phys.: Condens. Matter **2**, 701 (1990).
[2] F. de Groot and A. Kotani, *Core Level Spectroscopy of Solids* (Taylor and Francis, London, 2008).
[3] A. Shukla, M. Calandra, M. Taguchi, A. Kotani, G. Vanko, and S.-W. Cheong, Phys. Rev. Lett. **96**, 077006 (2006).
[4] C. Gougoussis, M. Calandra, A. Seitsonen, Ch. Brouder, A. Shukla, and F. Mauri, Phys. Rev. B **79**, 045118 (2009).
[5] A. Juhin, G. Calas, D. Cabaret, L. Galoisy, and J.-L. Hazemann, Phys. Rev. B **76**, 054105 (2007).
[6] P. Wernet, D. Nordlund, U. Bergmann, M. Cavalleri, M. Odelius, H. Ogasawara, L. A. Naslund, T. K. Hirsch, L. Ojamae, P. Glatzel, L. G. M. Pettersson, and A. Nilsson, Science **304**, 995 (2004).
[7] R. L. C. Wang, H. J. Kreuzer, and M. Grunze, Phys. Chem. Chem. Phys. **8**, 4744 (2006).
[8] J. D. Smith, C. D. Cappa, B. M. Messer, W. S. Drisdell, R. C. Cohen, and R. J. Saykally, J. Phys. Chem. B **110**, 20038 (2006).
[9] D. Prendergast and G. Galli, Phys. Rev. Lett. **96**, 215502 (2006).
[10] T. Head-Gordon and M. E. Johnson, Proc. Natl. Acad. Sci. U.S.A. **103**, 7973 (2006).

[11] G. Brancato, N. Rega, and V. Barone, Phys. Rev. Lett. **100**, 107401 (2008).
[12] R. D. Cowan, *The Theory of Atomic Structure and Spectra* (University of California Press, Berkeley, 1981).
[13] C. R. Natoli, D. K. Misemer, S. Doniach, and F. W. Kutzler, Phys. Rev. A **22**, 1104 (1980).
[14] L. Fonda, J. Phys.: Condens. Matter **4**, 8269 (1992).
[15] A. L. Ankudinov, B. Ravel, J. J. Rehr, and S. D. Conradson, Phys. Rev. B **58**, 7565 (1998).
[16] E. L. Shirley, Phys. Rev. Lett. **80**, 794 (1998).
[17] M. Taillefumier, D. Cabaret, A.-M. Flank, and F. Mauri, Phys. Rev. B **66**, 195107 (2002).
[18] P. E. Blöchl, Phys. Rev. B **50**, 17953 (1994).
[19] B. Hetényi, F. De Angelis, P. Giannozzi, and R. Car, J. Chem. Phys. **120**, 8632 (2004).
[20] C. J. Pickard and M. C. Payne, in *Electron Microscopy and Analysis 1997*, edited by J. M. Rodenburg, Vol. 153, pp. 179-182, Proceedings of the Institute of Physics Electron Microscopy and Analysis Group Conference, University of Cambridge (IOP, Bristol, 1997).
[21] P. Rez, J. R. Alvarez, and C. J. Pickard, Ultramicroscopy **78**, 175 (1999).
[22] S. P. Gao, C. J. Pickard, M. C. Payne, J. Zhu, and J. Yuan, Phys. Rev. B **77**, 115122 (2008).
[23] The presence of a core hole in the pseudopotential of the absorbing atom reduces the symmetry of the crystal.
[24] V. I. Anisimov, J. Zaanen, and O. K. Andersen, Phys. Rev. B **44**, 943 (1991).
[25] D. Vanderbilt, Phys. Rev. B **41**, 7892 (1990).
[26] The solutions of the radial Schrödinger equations for the isolated atom are a natural choice for the all-electron partial waves.
[27] J. R. Yates, C. J. Pickard, and F. Mauri, Phys. Rev. B **76**, 024401 (2007).
[28] C. Lanczos, J. Res. Natl. Bur. Stand. **49**, 33 (1952).
[29] C. Lanczos, J. Res. Natl. Bur. Stand. **45**, 255 (1950).
[30] R. Haydock, V. Heine, and M. J. Kelly, J. Phys. C **5**, 2845 (1972).
[31] R. Haydock, V. Heine, and M. J. Kelly, J. Phys. C **8**, 2591 (1975).
[32] P. J. Hasnip and C. J. Pickard, Comput. Phys. Commun. **174**, 24 (2006).
[33] B. Walker and R. Gebauer, J. Chem. Phys. **127**, 164106 (2007).
[34] P. Giannozzi *et al.*, http://www.quantum-espresso.org
[35] J. P. Perdew, K. Burke, and M. Ernzerhof, Phys. Rev. Lett. **77**, 3865 (1996).
[36] The XSPECTRA package by C. Gougoussis, M. Calandra, A. Seitsonen, and F. Mauri is available under the GNU license in the current CVS version of the Quantum ESPRESSO code.
[37] Ch. Brouder, M. Alouani, and K. H. Bennemann, Phys. Rev. B **54**, 7334 (1996).
[38] G. A. Lager, J. D. Jorgensen, and F. J. Rotella, J. Appl. Phys. **53**, 6751 (1982).
[39] H. M. Otte, J. Appl. Phys. **32**, 1536 (1961).
[40] C. T. Chantler, C. Q. Tran, Z. Barnea, D. Paterson, D. J. Cookson, and D. X. Balaic, Phys. Rev. A **64**, 062506 (2001).
[41] Y. Joly, Phys. Rev. B **63**, 125120 (2001).
[42] M. Reehuis, C. Ulrich, K. Prokes, A. Gozar, and G. Blumberg, Seiki Komiya, Yoichi Ando, P. Pattison, and B. Keimer, Phys. Rev. B **73**, 144513 (2006).
[43] M. Cococcioni and S. de Gironcoli, Phys. Rev. B **71**, 035105 (2005).
[44] H. J. Kulik, M. Cococcioni, D. A. Scherlis, and N. Marzari, Phys. Rev. Lett. **97**, 103001 (2006).
[45] J. M. Ginder, M. G. Roe, Y. Song, R. P. McCall, J. R. Gaines, E. Ehrenfreund, and A. J. Epstein, Phys. Rev. B **37**, 7506 (1988).
[46] D. Vaknin, S. K. Sinha, D. E. Moncton, D. C. Johnston, J. M. Newsam, C. R. Safinya, and H. E. King, Phys. Rev. Lett. **58**, 2802 (1987).
[47] H. Tolentino, M. Medarde, A. Fontaine, F. Baudelet, E. Dartyge, D. Guay, and G. Tourillon, Phys. Rev. B **45**, 8091 (1992).
[48] R. A. Bair and W. A. Goddard, Phys. Rev. B **22**, 2767 (1980).
[49] N. Kosugi, Y. Tokura, H. Takagi, and S. Uchida, Phys. Rev. B **41**, 131 (1990).
[50] I. Yamada, A. A. Belik, M. Azuma, S. Harjo, T. Kamiyama, Y. Shimakawa, and M. Takano, Phys. Rev. B **72**, 224503 (2005).